

# RADIOCARBON



**CAMBRIDGE**  
UNIVERSITY PRESS

## **Inference from large sets of radiocarbon dates: software and methods**

Journal:	<i>Radiocarbon</i>
Manuscript ID	RDC-RES-2019-0037.R3
Manuscript Type:	Research Article
Date Submitted by the Author:	18-Jun-2020
Complete List of Authors:	Crema, Enrico Ryunosuke; University of Cambridge, Archaeology Bevan, Andrew; UCL, Institute of Archaeology
Keywords:	Radiocarbon dating, Summed Probability Distribution, Demography, Statistical analysis, Open Source Software
Abstract:	The last decade has seen the development of a range of new statistical and computational techniques for analysing large collections of radiocarbon dates, often but not exclusively to make inferences about human population change in the past. Here we introduce rcarbon, an open-source software package for the R statistical computing language which implements many of these techniques and looks to foster transparent future study of their strengths and weaknesses. In this paper, we review the key assumptions, limitations and potentials behind statistical analyses of summed probability distribution of radiocarbon dates, including Monte-Carlo simulation-based tests, permutation tests, and spatial analyses. Supplementary material provides a fully reproducible analysis with further details not covered in the main paper.

SCHOLARONE™  
Manuscripts

# 1 Inference from large sets of radiocarbon dates: software and methods

2

## 3 Abstract

4 The last decade has seen the development of a range of new statistical and computational techniques  
5 for analysing large collections of radiocarbon dates, often but not exclusively to make inferences about  
6 human population change in the past. Here we introduce *rcarbon*, an open-source software package for  
7 the R statistical computing language which implements many of these techniques and looks to foster  
8 transparent future study of their strengths and weaknesses. In this paper, we review the key assumptions,  
9 limitations and potentials behind statistical analyses of summed probability distribution of radiocarbon  
10 dates, including Monte-Carlo simulation-based tests, permutation tests, and spatial analyses.  
11 Supplementary material provides a fully reproducible analysis with further details not covered in the  
12 main paper.

13

## 14 1. Introduction

15 The last few years has seen a dramatic increase in the number of research projects constructing proxy  
16 time series of demographic change out of large lists of archaeological radiocarbon dates. Put simply,  
17 this approach assumes that, given a large enough set of radiocarbon dates taken on anthropogenic  
18 samples, then the changing frequency of dates through time will preserve a signal of highs and lows in  
19 past human activity and, by extension, in human population. Rick's (1987) work was pioneering in this  
20 regard, being the first to propose the key assumption that more people in a given chronological period  
21 would typically lead to more anthropogenic products entering the archaeological record in that period,  
22 implying more potential samples to date and ultimately more published radiocarbon dates. He also  
23 already noted the presence of biases that were likely to distort such a signal (1987: fig.1). While early  
24 experiments with such methods sometimes considered a histogram of uncalibrated conventional  
25 radiocarbon ages, researchers have since turned to the summation of the posterior probability  
26 distributions of calibrated dates, and the result has become commonly known as a summed probability  
27 distribution (hereafter SPD, although there have also been alternative names and formulations).

28

29 The sharply increasing popularity of SPDs over the last decade or so has rightly also prompted criticism,  
30 not only with regard to the overall inferential assumptions behind the idea, but also with respect to the  
31 viability of particular SPD-based analytical methods. For example, several researchers have emphasised  
32 the fact that the sampling intensity of radiocarbon dates might not be constant over time. A good  
33 example is the difference between the popularity of radiocarbon sampling in early Mediterranean  
34 prehistory (e.g. Mesolithic-Neolithic) versus its almost complete avoidance for the Greek or Roman  
35 periods of the same region, even though the latter was manifestly a period of considerable population  
36 (Palmisano et al 2017). In addition to the impact of this differing prioritisation of absolute versus relative  
37 dating by archaeologists working on different time periods, researchers have further suggested that  
38 different kinds of societies (of otherwise roughly similar population size, for instance) might  
39 conceivably produce different radiocarbon footprints and/or that, even if a correlation between dates  
40 and population exists, that these might not scale in a linear fashion (Freeman et al. 2017). Others have  
41 noted that there might be a taphonomic bias towards the preservation of more anthropogenic material  
42 from sites of later periods (Surovell and Brantingham 2007; Surovell et al. 2009), again implying that  
43 over extended periods of thousands of years, we should probably assume a non-linear scaling to human  
44 activity. Such critiques are often valid to some degree and focus on how we should interpret summed  
45 probability distributions of radiocarbon dates in the first place (see discussions in Contreras and

46 Meadows 2014; Morkkonen 2014; Tallavara et al 2014; Attenbrow and Hiscock 2015; Hiscock and  
47 Attenbrow 2016; Smith 2016; Williams and Ulm 2016) Indeed, some of these very same issues also  
48 apply to other attempts to reconstruct past population (e.g. settlement counts where again it is sometimes  
49 difficult to compare evenly across periods and regions).

50  
51 SPDs however also face a further challenge at a more fundamental level with regard to how best we  
52 might measure the changing frequencies of radiocarbon dates through time. Because calibrated  
53 radiocarbon dates comprise probability distributions spread across multiple calendar years and not  
54 discrete single estimates, the visual interpretation of aggregated SPDs becomes challenging and very  
55 often misleading at multiple scales. Peaks and troughs in SPDs might reflect changes in date intensity  
56 through time (and hence interpreted as population ‘booms’ or ‘busts’), but they might also be a  
57 consequence of the changing steepness of the calibration curve, the size of the dates’ associated  
58 measurement errors and/or just a statistical fluke from small sample sizes. In response to these  
59 challenges, a number of studies (Shennan and Edinborough 2007; Shennan et al. 2013; Timpson et al.  
60 2014; Crema et al. 2016; Bevan et al 2017; Bronk Ramsey 2017; Brown 2017; Crema et al. 2017;  
61 Edinborough et al. 2017; Freeman et al. 2018; McLaughlin 2018; Roberts et al. 2018) have developed  
62 new techniques to address some of these issues. Most notably, they have offered new approaches to the  
63 problem of discerning genuine fluctuations in the density of radiocarbon dates as opposed to statistical  
64 artefacts arising from sampling error, the calibration process or taphonomic histories. Even so,  
65 replication and reuse of such methods remains limited, due both to an understandable experimentation  
66 across multiple software packages for calibration and statistical analysis (e.g. OxCal, CalPal, and in  
67 various forms via the R statistical environment, see **Supplementary Figure 1**) and to only patchy  
68 provision, so far, of transparent and reproducible workflows.

69  
70 With a view to exploring and alleviating some of these issues, as well as with an eye to an increasing  
71 emphasis across archaeology and many other subjects on reproducible research (see Marwick 2016;  
72 Marwick et al 2017), we have recently developed *rcarbon* as an extension package for *R* (R Core Team  
73 2018), one of the most popular software environments for statistical computing. The *rcarbon* package  
74 provides basic calibration, aggregation, and visualisation functions comparable to those that exist in  
75 other software packages, but also offers a suite of further functions for simulation-based statistical  
76 analysis of SPDs. This paper will discuss the main features of *rcarbon*, will highlight technical details  
77 and their implications in the creation and analyses of SPDs, and will offer some additional thoughts on  
78 the strengths and weakness of SPD-based methods overall.<sup>1</sup>

## 79 2. Calibration and Aggregation

### 80 2.1 Basic Treatment: Calibration and Summation

81 In its most basic form an SPD extends the idea of a plotting a simple histogram of either uncalibrated  
82 <sup>14</sup>C ages or median calibrated dates to represent changing density of radiocarbon samples over time.  
83 Hence, the construction of an SPD involves two steps: (1) radiocarbon dates are calibrated so that for  
84 each sample we obtain a distribution of probabilities that the sample in question belongs to a particular

---

<sup>1</sup> Readers interested in applying these techniques on their own data are encouraged to read the R vignette associated with the package (<https://cran.r-project.org/web/packages/rcarbon/vignettes/rcarbon.html>). The supplementary material contains additional commentary and scripts for reproducing the analysis in the main paper. A copy of the supplementary material can also be accessed from the following repository: [https://github.com/ercrema/rcarbon\\_paper\\_esm](https://github.com/ercrema/rcarbon_paper_esm).

85 calendar year; and (2) all of these per-year probabilities are summed.<sup>2</sup> The resulting curve thus no longer  
 86 represents probabilities, but instead is taken as a measure of date intensity. The rationale is thus not  
 87 dissimilar to intensity-based techniques such as a univariate kernel density estimate (KDE), although  
 88 with a crucial difference. In the case of KDE, individual kernels associated to each sample have all the  
 89 same shape defined by the kernel bandwidth, itself mathematically estimated. In contrast, in the case of  
 90 SPDs, the probability distributions associated with each radiocarbon date have different shapes  
 91 depending on measurement error and the particularities of the relevant portion of the calibration curve.  
 92 Consequently, SPDs are not explicitly and straightforwardly an estimate of the underlying distribution  
 93 from which the observations are sampled from, and its absolute values cannot be directly compared  
 94 across datasets. It follows that their visual interpretation within and across datasets is intrinsically biased.

95

96 Basic calibration in *rcarbon* is conducted with reference either to one of the established marine or  
 97 terrestrial calibration curves or to a user-specific custom curve (in what follows, IntCal13 is used  
 98 throughout: Reimer et al. 2013). The arithmetic method is for all intents and purposes identical to the  
 99 the one adopted by OxCal (Bronk Ramsay 2008; leaving aside for a moment the more sophisticated  
 100 Bayesian routines the latter package uses for more complex phase modelling), and very similar to that  
 101 used by most other calibration software (Weninger et al 2015; Parnell 2018). Some of the terminology  
 102 used by *rcarbon*'s standard routine has also been made consistent with *Bchron*, a well-known R package  
 103 for handling radiocarbon dates and modelling pollen core chronologies and other age-depth  
 104 relationships (Haslett and Parnell 2008; Parnell 2018; see also the *clam* package; Blaaw 2019). In  
 105 *rcarbon*, the raw data stored for any given calibrated date consists of probability values per calibrated  
 106 calendar year BP (but convertible to other calendars such as BC/AD), and it is these per-year  
 107 probabilities that get summed to produce an SPD. For example, **Figure 1a** shows the result of adding  
 108 up 130 dates from the Neolithic flint mines of Grimes Graves, Norfolk with three individual dates shown  
 109 on top (for a full set and and more recent dates from the site, see Healy et al. 2014). A final point to  
 110 note is that many studies apply a final 'smoothing function' to the SPD (e.g. Kelly et al 2013, Timpson  
 111 et al 2014, Crema et al 2016, etc.), such as a running mean of between 50 and 200 years, to limit possible  
 112 artefacts resulting from sampling error (but also from the effects of the calibration process) and  
 113 discourage over-interpretation of the results (in **Figure 1a** an example with a 50-year running mean is  
 114 shown). We return to the pros and cons of such smoothing in what follows.

115

116

### 117 2.2 Phase or Site Over-Representation: Thinning and Binning

118 In most instances, rather than the single site example provided above, an SPD is constructed across a  
 119 wider region and using more than one site. As a result, there are further potential biases arising from  
 120 the fact that not all sites (or indeed site phases) may have received equivalent levels of investment in  
 121 radiocarbon dating. The Neolithic flint mining site of Grimes Graves in south-eastern England, for  
 122 instance, has received an unusual level of investment in dating compared to other British prehistoric  
 123 sites, but such differences do not accurately reflect a site's relative size or longevity of use. The  
 124 cumulative effect of these differences in inter-site sampling intensity, and in particular the presence of  
 125 abnormally high levels of sampling intensity of particular contexts, could thus generate artificial signals  
 126 in the SPD. While the ideal approach to the problem is to select only samples referring to specific types  
 127 of events (e.g. the construction of residential features) and control for sampling intensity via Bayesian  
 128 inference (e.g. using OxCal's *R\_Combine* function), the use of larger datasets with heterogeneous  
 129 samples makes this solution unfeasible.

---

<sup>2</sup> In some software (e.g. CalPal), these two steps can be reversed (uncalibrated dates are summed and then the resulting aggregate is calibrated in one go), and we discuss the implications of this further below.

130  
 131 There are two alternative approaches to account for heterogeneity in sampling intensity. The first one  
 132 involves manually going through a list of radiocarbon dates and choosing only a maximum number of  
 133 better (e.g. short-lived, low-error) dates per phase or per site. In *rcarbon*, this thinning approach can  
 134 also be achieved (in a less attentive but more automatic manner) using the *thinDates* function which  
 135 either selects a maximum subset of dates at random or with a mixed approach that allows for some  
 136 prioritisation of dates with lower errors (**Figure 1b**). This approach effectively replaces a set of  
 137 radiocarbon dates referring to the same “event” with a smaller subset with user-defined size and  
 138 inclusion criteria. As a consequence, the potentially biased contribution to the SPD of events associated  
 139 with a larger number of radiocarbon dates can be reduced. A second solution to reduce the potential  
 140 effect of such bias is to aggregate samples from the same site that are close in time, sum their  
 141 probabilities, and divide the resulting SPD by the number of dates. Such site or phase-level ‘binning’  
 142 was introduced by Shennan et al. (2013) and discussed in detail by Timpson et al. (2014). The rationale  
 143 is effectively to generate a local SPD referring to a particular occupation phase and to normalise this  
 144 curve to unity to reduce the impact of heterogeneous sampling intensity. The *rcarbon* package provides  
 145 a routine (*binPrep*), similar but not identical to the ones used in those two discussions, whereby dates  
 146 from the same sites are grouped based on their (uncalibrated or median calibrated) inter-distances in  
 147 time, defined by the parameter  $h$ , and then put into bins. Dates within the same bins are then aggregated  
 148 to produce a local SPD that is normalised to sum to unity before being aggregated with other dates (and  
 149 local SPDs) to produce the final curve. .

150  
 151 Different authors have already used different values for  $h$  (or comparable parameters) ranging anywhere  
 152 from 50 to 200 years (e.g. Shennan et al. 2013; Timpson et al. 2014; Crema et al. 2016; Bevan et al.  
 153 2017; Roberts et al. 2018). These choices can have a considerable effect on the resulting shape of the  
 154 within site or within-phase local SPD, with higher values effectively leading to a more spread-out  
 155 distribution of probabilities (**Figures 1c-e**) and we recommend exploring the implications of this  
 156 empirically (e.g. via the *binSense* routine in *rcarbon* package (see also Riris 2018). It is also worth  
 157 noting that there has been little or no discussion on what exactly constitutes a *bin* (or the “event” on  
 158 which the thinning procedure is based), and how this might differ as a function of  $h$ , and ultimately  
 159 affect the interpretation of SPDs. For example, *bins* generated from larger values of  $h$  effectively lead  
 160 to an equal contribution of (potentially differently sized) sites to the SPD, effectively making this a  
 161 proxy of site density rather than population size.

162

[ Figure 1 Here ]

164 *Figure 1. Summing, thinning and binning: (a) a summed probability distribution of dates from one site only (n=130 dates), with a slightly*  
 165 *smoothed version also shown, as well as three example dates, followed by comparison of the smoothed raw density with (b) a randomly*  
 166 *‘thinned’ dataset of just 10 dates from the same site, (c-e) binned datasets at clustering cut-offs of h=50, 100 and 200 respectively.*

### 167 2.3 Normalised vs Unnormalised dates

168 It is well-known that the shapes of individual calibrated probability distributions vary depending on the  
 169 steepness or flatness of the calibration curve at that point in time. Less well-known is the fact that the  
 170 area-under-the-curve of a date, calibrated in the usual arithmetic way, will not immediately sum to  
 171 unity, but instead is typically normalised to ensure that it does (i.e. by dividing by the total sum under  
 172 the curve for that date). **Figures 2a-b** provide two examples of dates at flat and steep portions of the  
 173 calibration curve respectively which produce dramatically different areas-under-the-curve before  
 174 normalisation. Weninger et al. (2015) first noted that the presence of this normalising correction  
 175 explains the ‘artificial spikes’ noted by several different studies of SPDs, in which such spikes occurred  
 176 in predictable ways at steep portions of the calibration curve (and which sometimes prompted attempts

177 to smooth them away via fairly aggressive moving averages and/or various forms of kernel density  
 178 estimate (see Williams 2012; Shennan et al. 2013; Timpson et al. 2014; Brown 2015, 2017; Ramsey  
 179 2017; McLaughlin 2018). **Figures 2c-e** provide three globally wide-ranging examples from the  
 180 literature of datasets where spikes have been observed, with those spikes being particularly pronounced  
 181 in early Holocene time series. In contrast, when unnormalised dates are summed, such spikes are not  
 182 present. On first consideration, it is tempting to deem the normalised dates more theoretically justifiable,  
 183 regardless of the spikes, because each date is seemingly ‘treated equally’ (i.e. each has a weight of 1 in  
 184 the summation). However, because the summing a set of unnormalised calibrated dates (with varying  
 185 post calibration areas under the curve) produces exactly the same result as first summing a set of  
 186 uncalibrated Gaussians conventional radiocarbon age distributions (each of unity weight) and then  
 187 calibrating them in one go (the process in *CalPal*, and also achievable in *rcarbon*, although not the  
 188 default: see **Supplementary Figure 2**), this theoretical premise of the ‘equal treatment’ of each sample  
 189 (i.e. the issue of unnormalised dates yielding an area under the curve equal to unity) can in fact be  
 190 argued both ways (see Weninger et al. 2015 for extensive discussion). Regardless, these issues urge a  
 191 basic caution not to over-interpret SPD results without considerable attention to how individual highs  
 192 and lows in the data may have arisen.

193 [Figure 2 Here]

194 *Figure 2. Comparisons of unnormalised and normalised dates and their consequences: (a) a single date at a flat portion of the calibration*  
 195 *curve (area under the probability histogram: 1.337), (b) a single date at a steep portion of the calibration curve (area under the probability*  
 196 *histogram: 0.452), (c) Southern Levantine SPD ( $n_{\text{dates}} = 657$ ,  $n_{\text{sites}} = 119$ ,  $n_{\text{bins}} = 413$ ; data from Roberts et al 2018), (d) Sahara SPD ( $n_{\text{dates}} =$   
 197  $643$ ,  $n_{\text{sites}} = 233$ ,  $n_{\text{bins}} = 551$ ; data from Manning and Timpson 2014), and (e) Brazil SPD ( $n_{\text{dates}} = 173$ ,  $n_{\text{sites}} = 97$ ,  $n_{\text{bins}} = 171$ ; data from Bueno*  
 198 *et al 2013). The orange bar highlights time-intervals associated with steeper portions of the calibration curve.*

### 199 3. Statistical Testing

200 While it is tempting to treat the SPD itself as an unproblematic end goal with which to make  
 201 interpretations about past population dynamics, this is rarely true, and it is almost always important to  
 202 pay additional analytical attention to a host of uncertainties that come with it. For example, aside from  
 203 the concerns often voiced about whether the density of radiocarbon dates can be regarded as a reliable  
 204 proxy (see above), it is also worth noting at least two more issues. First, an ordinary SPD does not depict  
 205 the uncertainty associated with the fact that certain calendar years are more likely to accrue a more  
 206 narrowly defined dated sample than others (see **Supplementary Figure 3** for a worked through  
 207 example). Nor does it depict the further uncertainty associated with larger or smaller sample sizes of  
 208 dates or their measurement errors. A large number of radiocarbon dates for a given study may well  
 209 improve the chance of a good signal, but there is no magic threshold, as this depends very much on the  
 210 scope and goals of the analysis (e.g. inferences about multi-millennial trends versus those about sub-  
 211 millennial trends, inferences about perceived growth rates through time or instead about regional  
 212 differences across geographic space).

213

#### 214 3.1 Model Fitting and Hypothesis Testing

215 There have been various attempts so far to address these uncertainties, most of them leveraging the  
 216 flexibility of Monte Carlo-type conditional simulation in some fashion, although more formally  
 217 Bayesian models have also been proposed (see final section). Perhaps the most well-known approach  
 218 was introduced by Shennan et al (2013) and compares an observed SPD with a theoretical null  
 219 hypothesis of population change, where the latter might for instance imply stability (e.g. a flat, uniform  
 220 theoretical SPD), growth (e.g. an exponential theoretical model) or initial growth-and-plateau (e.g. a  
 221 logistic model) to name just a few of the most common (e.g. Shennan et al 2013; Crema et al. 2016;  
 222 Bevan et al. 2017, Fernández-López de Pablo et al 2019). The usual workflow involves (1) fitting such  
 223 a theoretical model to the observed SPD, (2) drawing  $s$  dates proportional to the shape of this fitted

224 model (where  $s$  matches the number of observed dates or the number of bins if the dates have been  
225 binned), (3) back-calibrating individual dates from calendar time to  $^{14}\text{C}$  age, and assigning an error to  
226 each by randomly sampling (with replacement) the observed  $^{14}\text{C}$  age errors in the input data, (4)  
227 generating a theoretical SPD from the simulated data obtained in steps 2 and 3(5) repeating steps 2-4  $n$   
228 times and generating a critical (e.g. 95%) envelope for the theoretical SPD given the sample size, and  
229 (6) computing the amount that the observed SPD falls outside the simulation envelope compared to the  
230 randomised runs to produce a global p-value (as extensively described by Timpson et al 2014). These  
231 general steps have separately implemented by several authors (Zahid et al. 2016; Crema et al. 2016;  
232 Porčić and Nikolić 2016; Silva and Vander Linden 2017) with some minor differences (e.g. the formula  
233 for calculating the p-value, screening for false positives, etc.), and effectively treats the observed SPD  
234 as something comparable to a test statistic.

235  
236 This approach has had the great virtue of grappling with the uncertainties associated with SPDs directly,  
237 but it is worth noting nevertheless that the choice, fitting and simulation of a null model of this kind is  
238 not straightforward. First, there are non-trivial technical niceties to do with how such a model is fitted  
239 in terms of the error model (e.g. log-linear or non-linear), or the time interval over which the model is  
240 fitted versus the interval over which it is simulated (given that all SPDs suffer from edge effects at their  
241 start and end dates). Second and more importantly, a particular model of theoretical population change  
242 or stability has to be selected and justified on contextual grounds, with perhaps the idea of exponential  
243 growth carrying the most straightforward demographic assumptions (all other things being equal and in  
244 light of the very long-term trend towards higher global population densities that seems to support this),  
245 but with other models often providing better fit to data or allowing certain kinds of extrapolation (e.g.  
246 Silva and Vander Linden 2017). A final point to stress regards the general limitations associated with  
247 the whole null hypothesis-testing approach: with a large enough sample, it will always be possible to  
248 produce a ‘significant’ result, but this may not warrant the kind of interpretation archaeologists and  
249 others are often looking for (e.g. about population “booms” and “busts”). It is also worth noting that  
250 intervals identified as positive or negative deviations from the null model are based on the density of  
251 dates and not on the trajectory of growth or decline even though the latter may be more interpretatively  
252 relevant in many situations. This means that, for example, intervals with positive deviations might well  
253 include instances of a decline in the density of radiocarbon dates. The Monte-Carlo simulation  
254 framework can be easily adapted to take this into account, allowing for testing against growth rates (see  
255 **supplementary figure 4**). Finally, the 95% critical envelopes produced for assessments of localised  
256 departure of the observed SPD from a theoretical pattern or a second SPD (see below, figures 3-4 for  
257 examples) are indicators only and should not be read as a set of formal significance tests for all years  
258 as this runs the well-known risk of multiple testing (see Loosmore and Ford 2006: 1926, for similar  
259 issues associated with the Monte Carlo envelopes produced for spatial point pattern analysis).

260  
261 Many existing implementations of this technique both fit and sample from their theoretical models in  
262 calendar time. A set of individual calendar years are first drawn proportional to the fitted model, then  
263 these are back-calibrated individually to become a set of conventional (uncalibrated)  $^{14}\text{C}$  ages with small  
264 errors deriving from those associated with the calibration curve itself. Then, larger plausible error terms  
265 are added to mimic the instrumental measurement errors of the observed dates and each age (typically  
266 now a Gaussian probability distribution) is then calibrated back into calendar time before all of the  
267 simulated dates are then finally aggregated into an SPD. This procedure can be formally described by  
268 a marginal probability with the assumption of a discretized calendar timeline:

269  
270



$$271 \quad p(r) = \sum_t^T \text{Pr}(t) \times p(r|\mu_t, \sigma_t^2) \quad [1]$$

272  
273

274 where  $p(r)$  is the probability of selecting a random sample with a  $^{14}\text{C}$  age  $r$ ,  $\text{Pr}(t)$  is the probability  
275 obtained from the fitted theoretical model at the calendar year  $t$  within  $T$  points in time across the  
276 temporal window of analysis,  $\mu_t$  and  $\sigma_t$  are their corresponding date in  $^{14}\text{C}$  age and the associated error  
277 on the calibration curve, and  $p(r|\mu_t, \sigma_t)$  refers to the Gaussian probability density function. Thus, if we  
278 ignore binning, given an observed dataset with  $k$  radiocarbon dates and a theoretical model  $\text{Pr}(t)$ , one  
279 could apply equation 1 to obtain  $k$   $^{14}\text{C}$  ages, to which we can assign random instrumental measurement  
280 errors by resampling from the observed data.

281

282 The term  $\text{Pr}(t)$  is generally obtained by: 1) fitting a curve (via regression) to an observed SPD over a  
283 defined temporal window; and 2) transforming the fitted values (e.g. for each discrete calendar year) so  
284 they sum to unity. Shennan et al (2003) initially fitted an exponential curve (as a null expectation for  
285 population with a constant growth rate), but other models have also been applied subsequently (cf.  
286 Crema et al 2016, Bevan et al 2017). It is also worth noting that  $\text{Pr}(t)$  does not have to be based on  
287 observed SPDs, and could potentially be derived from theoretical expectations or other demographic  
288 proxies (see Crema and Kobayashi 2020 for an example).

289

290 The assumption behind this sampling and back-calibration procedure (referred to in *rcarbon* as the  
291 *calsample* method, due to its sampling in calendar time) is that it will directly emulate both the kinds  
292 of uncertainty associated with a given observed sample size, and the impact on an SPD of the non-  
293 linearities in the calibration curve itself. However, the relationship between calendar years and  
294 radiocarbon ages is not commutative in the way such an approach implies (in agreement with Weninger  
295 et al 2015), and major problems are encountered in certain narrow parts of the calendar timescale,  
296 coincident with the same zones of artificial spiking first described above. **Figures 3a-b** depict the  
297 problem for the later Pleistocene and earlier Holocene time-frame using the same dated as in **figure 2c**.  
298 As before, we can note the difference in terms of spiking observed at predictable portions of the  
299 calibration curve where such spikes are present if we normalise individual dates but absent if we do not.  
300 However, the simulated envelopes created by the *calsample* approach exhibit quite different statistical  
301 artefacts at these locations (slight, offset dips if dates are normalised and dramatic dips if they are not).  
302 In neither case, do they seem to emulate the observed patterns.

303

304 In contrast, one alternative for generating theoretical SPDs is to back-calibrate the entire fitted model  
305 in one go and then to weight the result  $p(r)$  by the expected probability of sampling  $r$  under a uniform  
306 model:

307

$$308 \quad v(r) = \frac{\sum_t^T \text{Pr}(t|null) \times p(r|\mu_t, \sigma_t^2)}{\sum_t^T \text{Pr}(t|uniform) \times p(r|\mu_t, \sigma_t^2)} \quad [2]$$

309

310 Here  $\text{Pr}(t|null)$  is the fitted model under the null hypothesis, and  $\text{Pr}(t|uniform)$  is the probabilities  
311 associated with a uniform distribution covering for the same temporal range  $T$ .  $v(r)$  is then normalised  
312 to unity:

313

$$w(r) = \frac{v(r)}{\sum_r^R v(r)} \quad [3]$$

315  
316 with  $R$  being all the  $^{14}\text{C}$  ages examined, most typically the range covered by the calibration curve.

317  
318 Simulations following this approach then draw samples of uncalibrated ages from the back-calibrated  
319 model and calibrate these, before summing (this is therefore referred to in *rcarbon* as the *uncalsample*  
320 method, see also Roberts et al 2018; Bevan et al 2017 for applications). The adjustment of the  
321 probability of sampling specific  $^{14}\text{C}$  ages according to a baseline uniform model allows for much better  
322 simulation of the presence and amplitude of artificial peaks in the SPD at steeper portions of the  
323 calibration curve when dates are normalised, and their absence when dates are left unnormalised  
324 (**Figures 3c-d**). However, we note that neither approach is likely to be ideal, and discuss some  
325 promising alternatives in the sections below.

326  
327 [Figure 3 Here]

328 *Figure 3: The relationship between observed data and simulations envelopes for four different methods (using the same data as in figure*  
329 *2c): calsample realisations of (a) normalised and (b) unnormalised dates, and uncalsample realisations of (c) normalised and (d)*  
330 *unnormalised dates. Temporal ranges highlighted in red and blue represent intervals where the observed SPD show a significant positive or*  
331 *negative deviation from the simulated envelope (they do not necessarily imply the onset point of significant growth or decline).*  
332

### 333 3.2 Comparison and Testing of Multiple SPDs

334 A key advantage of SPDs over more traditional proxies of prehistoric population change, such as  
335 settlement counts, is the greater ease with which trajectories across different geographical regions can  
336 be compared, without the analytically-awkward frameworks imposed by different relative artefact-  
337 based chronologies. With this in mind, Crema et al. (2016) developed a permutation-based test to  
338 statistically compare two or more SPDs. While the null hypothesis for the one-sample models discussed  
339 above is a user-supplied theoretical growth model (e.g. we should expect exponential population growth  
340 all other things being equal), the null hypothesis of the multi-sample approach is that the SPDs are  
341 samples derived from the same statistical population (e.g. there is no meaningful difference between  
342 the shape of the SPD for region A and the one for region B). As for the one-sample approach p-values  
343 are obtained via simulation, but in this case rather than generating samples from a theoretical fitted  
344 model, the label defining the membership of each date (or bin if binning is being used) is permuted (e.g.  
345 we shuffle which dates belong to group A and which ones belong to group B, then produce a new SPD  
346 for each group, and repeat many times). This approach can be used to compare SPDs from different  
347 regions (as in Crema et al. 2016; Bevan et al. 2017; Riris 2018; Roberts et al. 2018) in order to infer  
348 where local population dynamics differ significantly through time, but it can also be used to consider  
349 other groupings of dates, such as those taken on different kinds of physical radiocarbon sample (Bevan  
350 et al. 2017). Such a *mark permutation test* will generate simulation envelopes for each SPD whose width  
351 proportional to the sample size (i.e. the overall number of dates per region, or the overall number of  
352 bins if binning has been applied; **figure 4**). Similar to the case of the one-sample approach, both one  
353 global and a set of local p-values can be obtained, the former assessing whether there are significant  
354 overall differences between sets and the latter identifying particular portions of the SPD with important  
355 differences in the summed probabilities.

356

357 While there are certainly still ways to mis- or over-interpret the results of this kind of mark permutation  
 358 test, one major strength is that they do not face quite the same problems associated with model selection,  
 359 fitting and simulation that the one sample approach does.

360

361 [Figure 4 Here]

362 *Figure 4: Example of mark permutation test (Crema et al 2016), comparing the SPDs from Southern ( $n_{dates} = 657$ ,  $n_{sites} = 119$ ,  $n_{bins} = 413$ ) and*  
 363 *Northern Levant ( $n_{dates} = 589$ ,  $n_{sites} = 41$ ,  $n_{bins} = 296$ ). Temporal ranges highlighted in red and blue represents intervals where the observed*  
 364 *SPD show a significant positive or negative deviation from the pan-regional null model. Data from Roberts et al 2018.*

#### 365 4. Spatial Analysis

366 A regional mark permutation test such as described above already offers one way to compare different  
 367 geographic regions, but its application requires a crisp definition of these regions from the outset and it  
 368 is thus not a particularly flexible way to explore variation across continuously varying geographic  
 369 spaces. Early extensions of the SPD approach already had further spatial inferences in mind when they  
 370 made use of weighted kernel density estimates (KDE) to infer regions of high or low concentrations of  
 371 dates across multiple temporal slices, occasionally using animations (e.g. Collard et al 2010; Manning  
 372 and Timpson 2014). Such visual inspection can be the basis for developing specific hypotheses, but  
 373 suffers from the same limitations as a non-spatial SPDs: it is hard to know what to interpret as interesting  
 374 variation in date intensity, through time and space, versus variation introduced by the calibration process,  
 375 by sampling error or by investigative bias. Recent spatio-temporal analyses of radiocarbon dates have  
 376 tackled this issue in two distinct ways, and we consider each one in turn below.

377

##### 378 4.2 Flexible Timeslice Mapping

379 In *rcarbon*, for instance, it is possible to map the spatio-temporal intensity of observed radiocarbon  
 380 dates as relevant for a particular 'focal' year (using the *stkde* function). This is achieved by first  
 381 computing weights associated with each sampling point  $x$  given the 'focal' year  $f$  and temporal  
 382 bandwidth  $b$  using the following equation:

383

$$384 \quad w(x, f, b) = \sum_i^T p_i(x) e^{-\frac{(i-f)^2}{2b^2}} \quad [4]$$

385

386 where  $p_i(x)$  is the probability mass associated with the year  $i$  obtained from the calibration process. In  
 387 other words, a temporal Gaussian kernel is placed around a chosen year and then the degree of overlap  
 388 between this kernel and the probability distribution of each date is evaluated. Each georeferenced date  
 389 also has a Gaussian distance-weighted influence on spatial intensity estimate at a given location on the  
 390 map (with the help of the R package *spatstat*: Baddeley et al 2015): in other words, a spatio-temporal  
 391 kernel is applied, with both the spatial and the temporal Gaussian bandwidths defined by the user. The  
 392 choice of appropriate spatial and the temporal bandwidth can arise from data exploration which suggests  
 393 combinations that are both empirically-useful (e.g. for the particular problem or question of interest)  
 394 and practically-aware (e.g. of the positional and temporal uncertainties in the underlying data), or it can  
 395 be made via one of several automatic bandwidth selectors (see Davies et al 2018 for a specific review  
 396 tailored to spatio-temporal analysis). While the latter option has the advantage of avoiding somewhat  
 397 arbitrary values for the kernel bandwidth, it is worth noting that the choice of different bandwidth  
 398 selectors can lead to very different result, particularly in the context of spatio-temporal analysis where

399 there is no single agreed algorithm<sup>3</sup>. **Figure 5a** shows an example of the resulting surface for the focal  
 400 year 6000 calBP, while **figure 5b** shows an unchanging overall surface where all samples are treated  
 401 equally regardless of their actual date (i.e. an ordinary kernel density map).

402

403 **Figure 5c** shows the result of dividing one by the other which offers an indication of the *proportion* of  
 404 local dates belonging to the focal, target time period, thereby to some extent detrending for any recovery  
 405 biases present in the overall sample. This is analogous and consistent with the idea of *relative risk*  
 406 mapping (Kelsall and Diggle 1995; Bevan 2012) and such an approach has been used by Chaput et al  
 407 (2015) and Bevan et al (2017) to investigate spatial variation in the radiocarbon density North America  
 408 and in the British Isles respectively. **Figure 5d** shows a further and final useful measure is of ‘change’  
 409 between the focal year and some earlier reference or backsight year (e.g. 200 years before, with various  
 410 options for how ‘change’ or growth/decline is expressed). Colour ramps can be standardised to allow  
 411 comparison across time-slices and thus also animation through multiple timeslices.

412

413

[Figure 5 Here]

414

415

416

417

418

419

420

#### 4.2 Spatial Testing

421

422

423

424

425

426

427

428

429

430

431

432

433

434

435

436

437

438

439

440

441

442

443

444

## 5. Conclusion

As the above should make clear, we continue to see great promise in the aggregate treatment of radiocarbon dates as proxies for activity intensity, and it is interesting to note that similar conclusions have been made in other fields that do not focus on human population, but instead use such lists to explore, amongst other things, alluvial accumulation, volcanic activity or peat deposition (Micheczyńska and Pazdur 2004; Surovell et al. 2009; Macklin et al 2014). The basic notion behind an SPD remains relatively easy to understand and in part this is probably the reason for its widespread appeal, even if some of the ensuing testing methods become more complicated. The *rcarbon* package is an attempt to

<sup>3</sup> Users interested in applying these different bandwidth selectors are advised to consult the R packages *spatstat* (Baddeley et al 2015) and *sparr* (Davies et al 2018). For an archaeological review of univariate and bivariate bandwidth selectors see Baxter et al 1997. See also Bronk-Ramsay 2017 for an alternative approach to univariate KDE for radiocarbon dates.

445 provide a working environment within which to explore both the strengths and weaknesses of such an  
446 approach. There is also a useful transferability of SPD approaches to proxy time series constructed from  
447 other kinds of evidence, such as dendrochronological dates (Ljungqvist et al. 2018) or even  
448 traditionally-dated artefact datasets. Even so, there continues to be a real need to consider how  
449 alternatives, for example Gaussian mixtures (Parnell 2018), might offer superior and theoretically more  
450 coherent frameworks, and to grapple further with quantisation and calibration curve effects (Weninger  
451 and Clare 2018).

452

### 453 **Acknowledgments**

454 We would like to thank several colleagues with whom we have discussed many aspects of this paper,  
455 as well those who provided constructive feedback on the *rcarbon* package, in particular: Anna Bloxam,  
456 Kevan Edinborough, Alessio Palmisano, Peter Schauer, Stephen Shennan, Fabio Silva and Bernhard  
457 Weninger. We are also grateful to the three anonymous reviewers for their insightful comments on the  
458 manuscript. This project has received funding from the European Research Council (ERC) under the  
459 Horizon 2020 research and innovation programme (Grant Agreement No 801953). This material  
460 reflects only the authors' views and the Commission is not liable for any use that may be made of the  
461 information contained therein.

462

### 463 **References**

464

465 Attenbrow, V., Hiscock, P. 2015. Dates and demography: are radiometric dates a robust proxy for  
466 long-term prehistoric demographic change? *Archaeology in Oceania*, 50: 30–36.

467

468 Baddeley, A., Rubak, E., Turner, R. 2015. *Spatial Point Patterns: Methodology and Applications*  
469 *with R*. London: Chapman and Hall/CRC Press

470

471 Baxter, M.J., Beardah, C.C., Wright, R.V.S. 1997. Some Archaeological Applications of Kernel  
472 Density Estimates. *Journal of Archaeological Science*, 24: 347–354.

473

474 Bevan, A. 2012. Spatial methods for analysing large-scale artefact inventories. *Antiquity*, 86(332):  
475 492–506.

476

477 Bevan, A., Colledge, S., Fuller, D., Fyfe, R., Shennan, S., Stevens, C. 2017. Holocene fluctuations in  
478 human population demonstrate repeated links to food production and climate. *Proceedings of the*  
479 *National Academy of Sciences*, 114(49):E10524–E10531.

480

481 Blaauw M. 2019. clam: Classical Age-Depth Modelling of Cores from Deposits. R package version  
482 2.3.2, URL: <<https://CRAN.R-project.org/package=clam>>

483

484 Bronk Ramsey, C. 2008. Radiocarbon dating: revolutions in understanding, *Archaeometry* 50(2): 249–  
485 75.

486

487 Bronk Ramsey, C. 2017. Methods for Summarizing Radiocarbon Datasets. *Radiocarbon*, 59(6):  
488 1809–1833.

489

- 490 Brown, W. A. 2015. Through a filter, darkly: population size estimation, systematic error, and random  
491 error in radiocarbon-supported demographic temporal frequency analysis. *Journal of Archaeological*  
492 *Science*, 53: 133–147.
- 493  
494 Brown, W. A. 2017. The past and future of growth rate estimation in demographic temporal frequency  
495 analysis: Biodemographic interpretability and the ascendance of dynamic growth models. *Journal of*  
496 *Archaeological Science*, 80: 96–108.
- 497  
498 Chaput, M. A., Kriesche, B., Betts, M., Martindale, A., Kulik, R., Schmidt, V., Gajewski, K. 2015.  
499 Spatiotemporal distribution of Holocene populations in North America. *Proceedings of the National*  
500 *Academy of Sciences*, 112(39): 12127–12132.
- 501  
502 Collard, M., Edinborough, K., Shennan, S., Thomas, M. G. 2010. Radiocarbon evidence indicates that  
503 migrants introduced farming to Britain. *Journal of Archaeological Science*, 37(4): 866–870.
- 504  
505 Contreras, D. A., Meadows, J. 2014. Summed radiocarbon calibrations as a population proxy: a  
506 critical evaluation using a realistic simulation approach. *Journal of Archaeological Science*, 52, 591–  
507 608.
- 508  
509 Crema, E. R., Bevan, A., Shennan, S. 2017. Spatio-temporal approaches to archaeological  
510 radiocarbon dates. *Journal of Archaeological Science*: 87, 1–9.
- 511  
512 Crema, Enrico R., Habu, J., Kobayashi, K., Madella, M. 2016. Summed Probability Distribution of 14  
513 C Dates Suggests Regional Divergences in the Population Dynamics of the Jomon Period in Eastern  
514 Japan. *PLOS ONE*, 11(4): e0154809. DOI:10.1371/journal.pone.0154809
- 515  
516 Crema, E.R., Kobayashi, K. 2020. A multi-proxy inference of Jōmon population dynamics using  
517 bayesian phase models, residential data, and summed probability distribution of 14C dates. *Journal of*  
518 *Archaeological Science*: 117, 105136. DOI:10.1016/j.jas.2020.105136
- 519  
520 Davies, Tilman M., Jonathan C. Marshall, and Martin L. Hazelton. (2018) Tutorial on Kernel  
521 Estimation of Continuous Spatial and Spatiotemporal Relative Risk. *Statistics in Medicine*, 37(7):  
522 1191-1221
- 523  
524 Edinborough, K., Porčić, M., Martindale, A., Brown, T. J., Supernant, K., Ames, K. M. 2017.  
525 Radiocarbon test for demographic events in written and oral history. *Proceedings of the National*  
526 *Academy of Sciences*, 114(47): 12436–12441.
- 527  
528 Fernández-López de Pablo, J., Gutiérrez-Roig, M., Gómez-Puche, M., McLaughlin, R., Silva, F.,  
529 Lozano, S., 2019. Palaeodemographic modelling supports a population bottleneck during the  
530 Pleistocene-Holocene transition in Iberia. *Nature Communications*, 10: 1872(2019). DOI:  
531 /10.1038/s41467-019-09833-3
- 532  
533 Freeman, J., Baggio, J. A., Robinson, E., Byers, D. A., Gayo, E., Finley, J. B., Meyer, J.A., Kelly,  
534 R.L., Anderies, J.M. 2018. Synchronization of energy consumption by human societies throughout  
535 the Holocene. *Proceedings of the National Academy of Sciences*, 115(40): 9962-9967.
- 536

- 537 Freeman, J., Byers, D. A., Robinson, E., Kelly, R. L. 2017. Culture Process and the Interpretation of  
538 Radiocarbon Data. *Radiocarbon*, 60(2): 453-467.
- 539
- 540 Haslett, J., Parnell, A.C., 2008. A simple monotone process with application to radiocarbon-dated  
541 depth chronologies, *Journal of the Royal Statistical Society: Series C Applied Statistics* 57.4: 399-418.
- 542
- 543 Hiscock, P., Attenbrow, V., 2016. Dates and demography? The need for caution in using radiometric  
544 dates as a robust proxy for prehistoric population change. *Archaeology in Oceania*, 51(3): 218–219.
- 545
- 546 Healy, F., Marshall, P., Bayliss, A., Cook, G., Bronk Ramsey, C., van der Plicht, J., Dunbar, E. 2014.  
547 *Grime's Graves, Weeting-with-Broomhill, Norfolk. Radiocarbon Dating and Chronological*  
548 *Modelling*, Portsmouth: Historic England Research Report 27/2014
- 549
- 550 Kelsall, J. E., Diggle, P. J. 1995. Non-parametric estimation of spatial variation in relative risk.  
551 *Statistics in Medicine*, 14(21–22): 2335–2342.
- 552
- 553 Ljungqvist, F.C., Tegel, W., Krusic, P.J., Seim, A., Gschwind, F.M., Haneca, K., Herzig, F.,  
554 Heussner, K.-U., Hofmann, J., Houbrechts, D., Kontic, R., Kyncl, T., Leuschner, H.H., Nicolussi, K.,  
555 Perrault, C., Pfeifer, K., Schmidhalter, M., Seifert, M., Walder, F., Westphal, T., Büntgen, U., 2018.  
556 Linking European building activity with plague history. *Journal of Archaeological Science* 98: 81–92.
- 557
- 558 Loosmore, N.B., Ford, E.D. 2006. Statistical inference using the G or K point pattern spatial statistics,  
559 *Ecology* 87: 1925-1931.
- 560
- 561 Macklin, M. G., Lewin, J., Jones, A.F. 2014. Anthropogenic alluvium: An evidence-based meta-  
562 analysis for the UK Holocene, *Anthropocene* 6: 26-38.
- 563
- 564 Marwick, B., 2017. Computational Reproducibility in Archaeological Research: Basic Principles and  
565 a Case Study of Their Implementation. *Journal of Archaeological Method and Theory*, 24: 424–450
- 566
- 567 Marwick, B., d'Alpoim Guedes, J., Barton, C. M., Bates, L. A., Baxter, M., Bevan, A., Bollwerk,  
568 E.A., Bocinsky, R.K., Brughmans, T., Carter, A.K., Conrad, C., Contreras, D.A., Costa, S., Crema,  
569 E.R., Daggett, A., Davies, B., Drake, B.L., Dye, T.S., France, P., Fullagar, R., Giusti, D., Graham, S.,  
570 Harris, M.D., Hawks, J., Heath, S., Huffer, D., Kansa, E.C., Kansa, S.W., Madsen, M.E., Melcher, J.,  
571 Negre, J., Neiman, F.D., Opitz, R., Orton, D.C., Przystupa, P., Raviele, M., Riel-Salvatore, J., Riris,  
572 P., Romanowska, I., Smith, J., Strupler, N., Ullah, I.I., Van Vlack, H.G., Van Valkenburgh, N.,  
573 Watrall, E.C., Webster, C., Wells, J., Winters, J., Wren, C.D. ,2017. Open Science in Archaeology,  
574 *SAA Archaeological Record*, 17: 8-14.
- 575
- 576 Michczyńska, D., Pazdur, A. 2004. Shape Analysis of Cumulative Probability Density Function of  
577 Radiocarbon Dates Set in the Study of Climate Change in the Late Glacial and Holocene.  
578 *Radiocarbon* 46(2): 733-744.
- 579
- 580 McLaughlin, T. R. 2019. On Applications of Space–Time Modelling with Open-Source 14C Age  
581 Calibration. *Journal of Archaeological Method and Theory*, 26: 479-501.
- 582
- 583 Mökkönen, T. 2014. Archaeological radiocarbon dates as a population proxy: a skeptical view.  
584 *Fennosc. Archaeol.* 31: 125-134.

- 585  
586 Parnell, A. 2018. Bchron: Radiocarbon Dating, Age-Depth Modelling, Relative Sea Level Rate  
587 Estimation, and Non-Parametric Phase Modelling, R package. URL: <[https://CRAN.R-](https://CRAN.R-project.org/package=Bchron)  
588 [project.org/package=Bchron](https://CRAN.R-project.org/package=Bchron)>  
589
- 590 Porčić, M., Nikolić, M. 2016. The Approximate Bayesian Computation approach to reconstructing  
591 population dynamics and size from settlement data: demography of the Mesolithic-Neolithic transition  
592 at Lepenski Vir. *Archaeological and Anthropological Sciences* 8(1): 169–186.  
593
- 594 R Core Team 2018. R: A language and environment for statistical computing. R Foundation for  
595 Statistical Computing, Vienna, Austria. URL: <<https://www.R-project.org/>>  
596
- 597 Reimer, P.J., Bard, E., Bayliss, A., Beck, J.W., Blackwell, P.G., Ramsey, C.B., Buck, C.E., Cheng,  
598 H., Edwards, R.L., Friedrich, M., Grootes, P.M., Guilderson, T.P., Haflidason, H., Hajdas, I., Hatté,  
599 C., Heaton, T.J., Hoffmann, D.L., Hogg, A.G., Hughen, K.A., Kaiser, K.F., Kromer, B., Manning,  
600 S.W., Niu, M., Reimer, R.W., Richards, D.A., Scott, E.M., Southon, J.R., Staff, R.A., Turney, C.S.M.,  
601 Plicht, J. van der, 2013. IntCal13 and Marine13 Radiocarbon Age Calibration Curves 0–50,000 Years  
602 cal BP. *Radiocarbon* 55: 1869–1887.  
603
- 604 Rick, J. W. 1987. Dates as Data: An Examination of the Peruvian Preceramic Radiocarbon Record.  
605 *American Antiquity*, 52: 55-73.  
606
- 607 Riris, P. 2018. Dates as data revisited: A statistical examination of the Peruvian preceramic  
608 radiocarbon record. *Journal of Archaeological Science*, 97: 67–76.  
609
- 610 Roberts, N., Woodbridge, J., Bevan, A., Palmisano, A., Shennan, S., Asouti, E. 2018. Human  
611 responses and non-responses to climatic variations during the last Glacial-Interglacial transition in the  
612 eastern Mediterranean. *Quaternary Science Reviews*, 184: 47–67.  
613
- 614 Shennan, S., Downey, S.S., Timpson, A., Edinborough, K., Colledge, S., Kerig, T., Manning, K.,  
615 Thomas, M.G., 2013. Regional population collapse followed initial agriculture booms in mid-  
616 Holocene Europe. *Nature Communications* 4: ncomms3486. DOI: 10.1038/ncomms3486.  
617
- 618 Shennan, S., Edinborough, K. 2007. Prehistoric population history: from the Late Glacial to the Late  
619 Neolithic in Central and Northern Europe. *Journal of Archaeological Science*, 34, 1339–1345.  
620 Silva, F., Vander Linden, M. 2017. Amplitude of travelling front as inferred from 14 C predicts levels  
621 of genetic admixture among European early farmers. *Scientific Reports*, 7(1): 11985.  
622 DOI:10.1038/s41598-017-12318-2  
623
- 624 Smith, M. 2016. The use of summed-probability plots of radiocarbon data in archaeology.  
625 *Archaeology in Oceania*, 51(3): 214–215.  
626
- 627 Surovell, T. A., Brantingham, P. J. 2007. A note on the use of temporal frequency distributions in  
628 studies of prehistoric demography. *Journal of Archaeological Science*, 34: 1868–1877.  
629
- 630 Surovell, T.A., Byrd Finley, J., Smith, G. M., Brantingham, P.J., Kelly, R. 2009. Correcting temporal  
631 frequency distributions for taphonomic bias, *Journal of Archaeological Science*, 36: 1715–1724.  
632



- 633 Tallavaara, M., Pesonen, P., Oinonen, M., Seppä, H. (2014). The mere possibility of biases does not  
634 invalidate archaeological population proxies—response to Teemu Mökkönen. *Fennosc. Archaeol*, 31:  
635 135-140.
- 636
- 637 Timpson, A., Colledge, S., Crema, E., Edinborough, K., Kerig, T., Manning, K., Thomas, M.G.,  
638 Shennan, S., 2014. Reconstructing regional population fluctuations in the European Neolithic using  
639 radiocarbon dates: a new case-study using an improved method. *Journal of Archaeological Science*  
640 52: 549–557.
- 641
- 642 Williams, A. N., & Ulm, S. 2016. Radiometric dates are a robust proxy for long-term demographic  
643 change: A comment on Attenbrow and Hiscock (2015). *Archaeology in Oceania*, 51(3): 216–217.
- 644
- 645 Weninger, B., Clare, L., Jöris, O., Jung, R., Edinborough, K. 2015. Quantum theory of radiocarbon  
646 calibration. *World Archaeology*, 47(4): 543–566.
- 647
- 648 Weninger B. and Clare L. 2018. High-Resolution Chronology of Shir, South Area, In Bartl K (ed.).  
649 *The Late Neolithic Site of Shir/Syria. Volume I. The Excavations at the South Area 2006–2009.*  
650 *Damaszener Forschungen, Vol. 18. Archaologische Forschungen in Syrien*: 183-198. Darmstadt:  
651 Philipp von Zabern.
- 652
- 653 Williams, A. N. 2012. The use of summed radiocarbon probability distributions in archaeology: a  
654 review of methods. *Journal of Archaeological Science*, 39, 578–589.
- 655
- 656 Zahid, H. J., Robinson, E., Kelly, R. L. 2016. Agriculture, population growth, and statistical analysis of  
657 the radiocarbon record. *Proceedings of the National Academy of Sciences*, 113(4): 931-935.

658

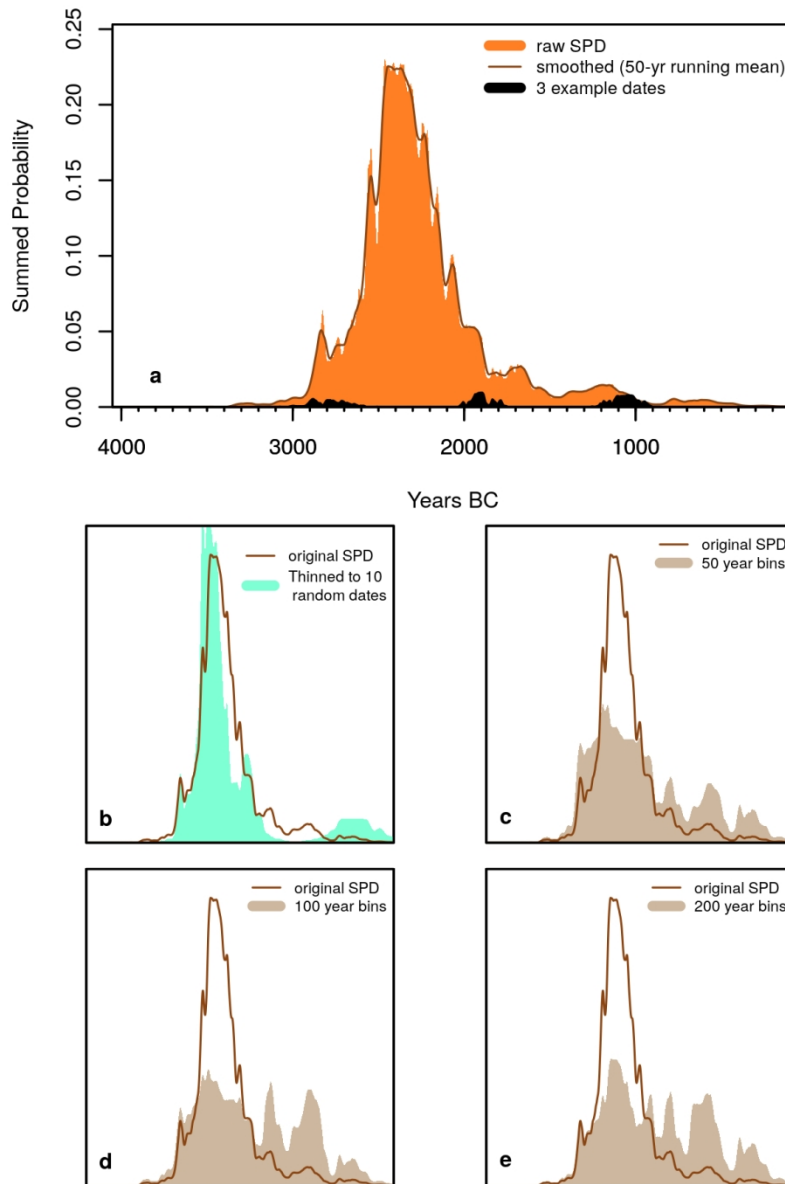


Figure 1. Summing, thinning and binning: (a) a summed probability distribution of dates from one site only ( $n=130$  dates), with a slightly smoothed version also shown, as well as three example dates, followed by comparison of the smoothed raw density with (b) a randomly 'thinned' dataset of just 10 dates from the same site, (c-e) binned datasets at clustering cut-offs of  $h=50$ , 100 and 200 respectively.

101x152mm (300 x 300 DPI)

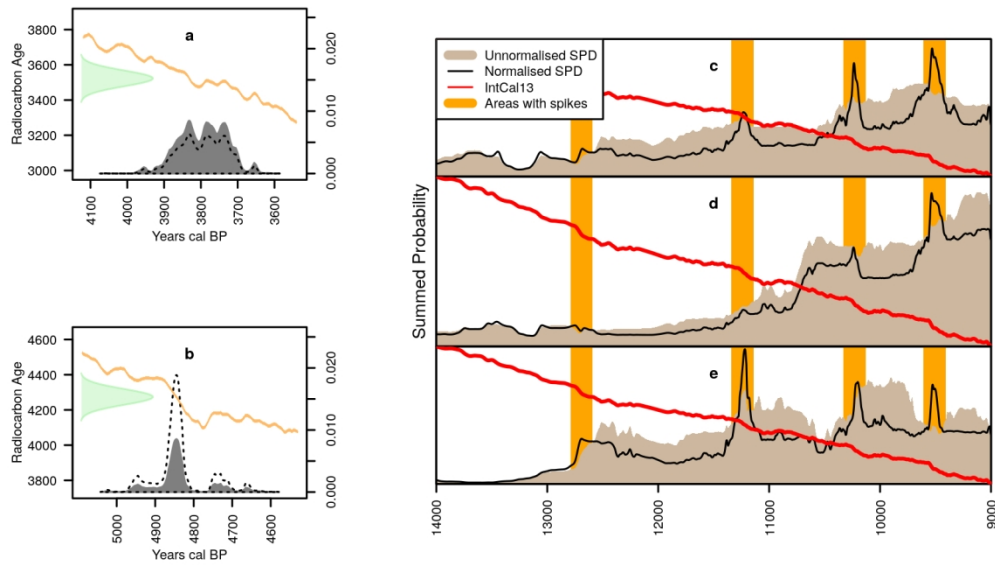


Figure 2. Comparisons of unnormalised and normalised dates and their consequences: (a) a single date at a flat portion of the calibration curve (area under the probability histogram: 1.337), (b) a single date at a steep portion of the calibration curve (area under the probability histogram: 0.452), (c) Southern Levantine SPD (ndates= 657, nsites= 119, nbins= 413 ; data from Roberts et al 2018), (d) Sahara SPD (ndates= 643, nsites= 233, nbins= 551 ; data from Manning and Timpson 2014), and (e) Brazil SPD (ndates= 173, nsites= 97, nbins= 171 ; data from Bueno et al 2013). The orange bar highlights time-intervals associated with steeper portions of the calibration curve.

139x88mm (300 x 300 DPI)

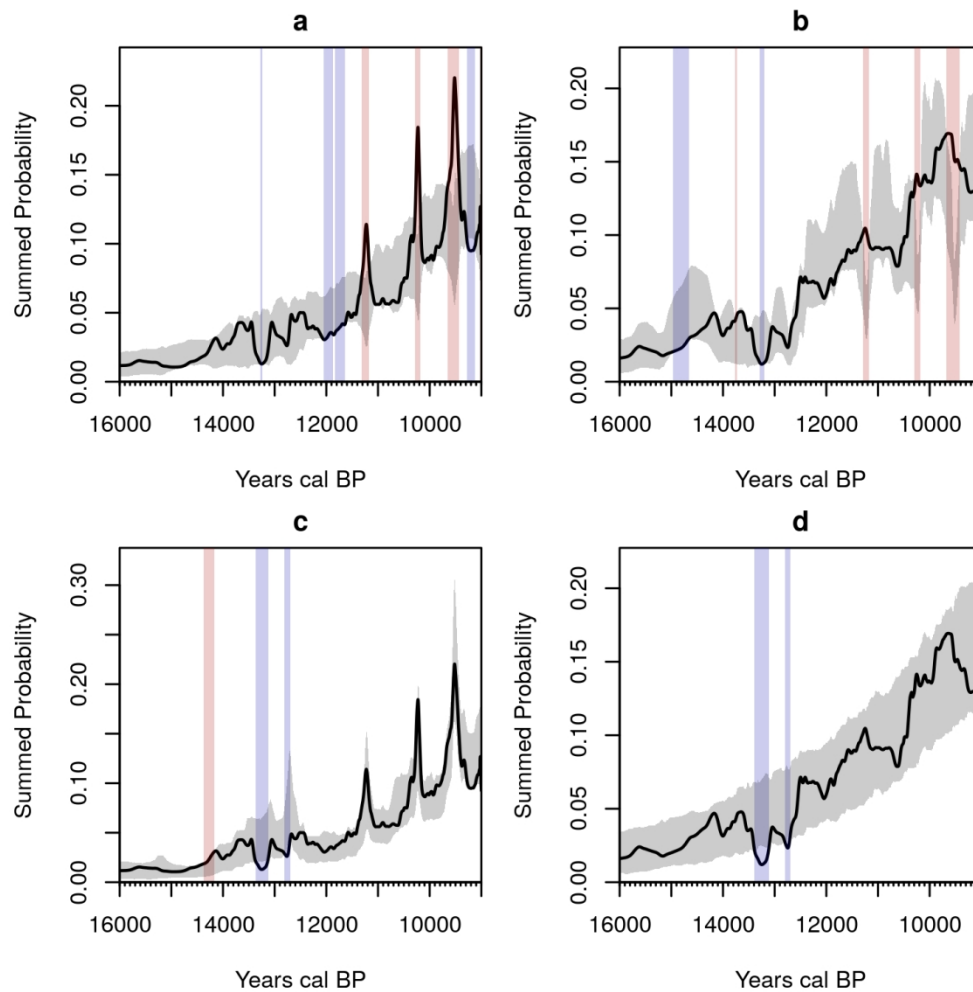


Figure 3: The relationship between observed data and simulations envelopes for four different methods (using the same data as in figure 2c): calsample realisations of (a) normalised and (b) unnormalised dates, and uncalsample realisations of (c) normalised and (d) unnormalised dates. Temporal ranges highlighted in red and blue represent intervals where the observed SPD show a significant positive or negative deviation from the simulated envelope (they do not necessarily imply the onset point of significant growth or decline).

127x127mm (300 x 300 DPI)

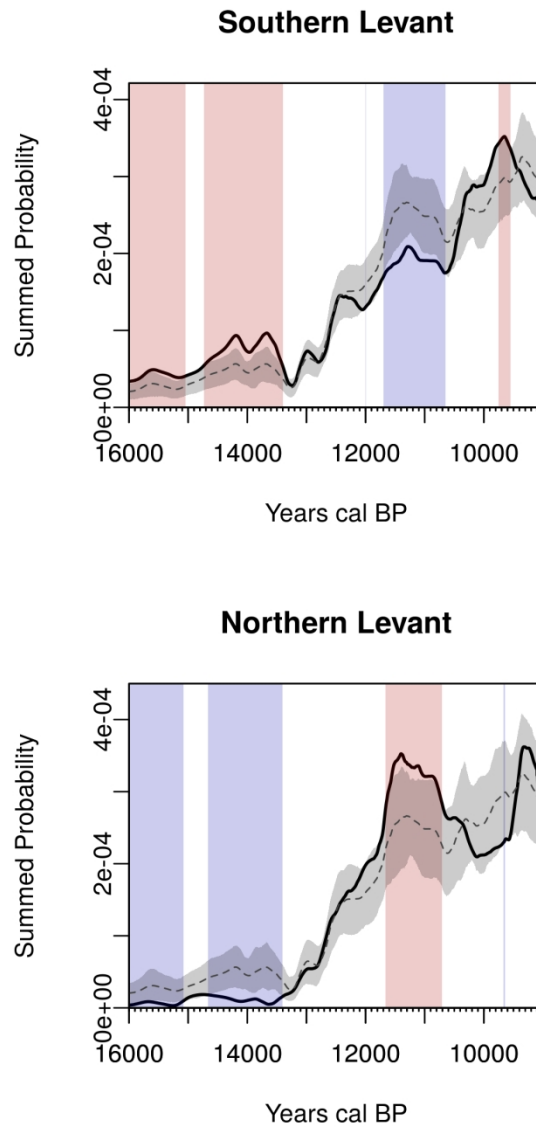


Figure 4: Example of mark permutation test (Crema et al 2016), comparing the SPDs from Southern (ndates= 657, nsites= 119, nbins= 413) and Northern Levant ( ndates= 589, nsites= 41, nbins= 296). Temporal ranges highlighted in red and blue represents intervals where the observed SPD show a significant positive or negative deviation from the pan-regional null model. Data from Roberts et al 2018.

101x203mm (300 x 300 DPI)

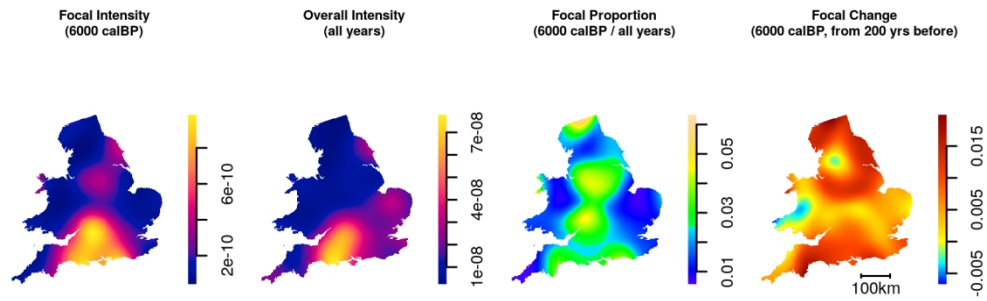


Figure 5. Example output of one focal year of a kernel density map of English and Welsh dates from the Euroevol Neolithic dataset ( $n_{\text{dates}}= 2,327$ ,  $n_{\text{sites}}= 653$ ,  $n_{\text{bins}}= 1,461$ , data from Manning et al 2016): (a) the spatio-temporal intensity for the focal year 6000 calBP, (b) the overall spatial intensity for Neolithic dates (8000-4000 calBP), (c) the proportion of a) out of b), and (d) a measure of the spatial pattern of change, mostly growth, from 6200 calBP to 6000 calBP.

139x50mm (300 x 300 DPI)

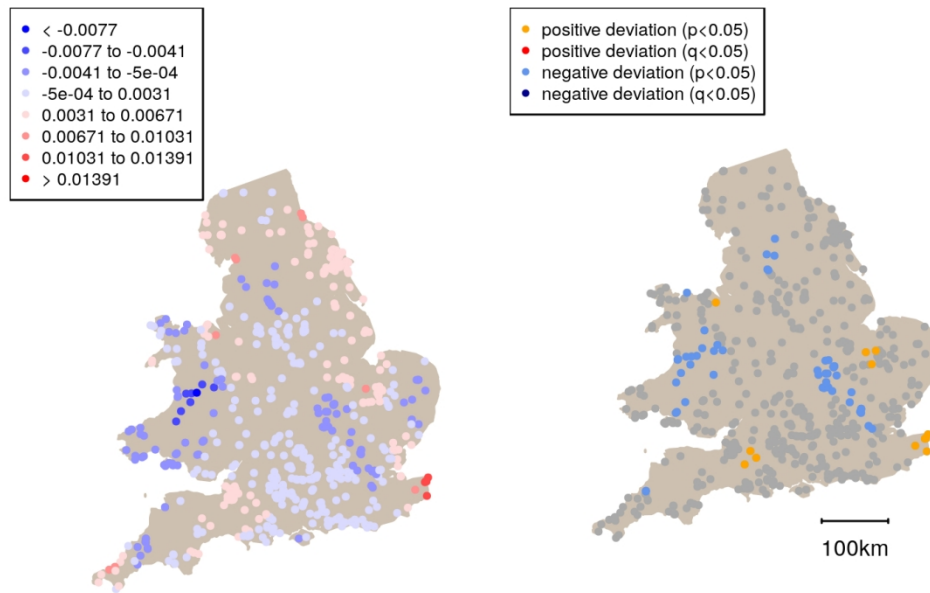


Figure 6. Spatial permutation test for the same data as figure 5 showing: (a) the local mean geometric growth rates mean geometric growth rate between 6300-6100 to 6100-5900 calBP; and (b) results of the spatial permutation test for the same interval showing local significant positive and negative significant departures from the null hypothesis.

127x88mm (300 x 300 DPI)